Journal of Molecular Catalysis A: Chemical 334 (2011) 116–122

Contents lists available at ScienceDirect

Journal of Molecular Catalysis A: Chemical

journal homepage: www.elsevier.com/locate/molcata

Efficient decomposition of organic compounds and reaction mechanism with BiOI photocatalyst under visible light irradiation

Yongyu Li, Jianshe Wang, Hongchang Yao, Liyun Dang, Zhongjun Li*

Department of Chemistry, Zhengzhou University, No. 100 of Science Road, Zhengzhou 450001, PR China

ARTICLE INFO

Article history:
Received 13 July 2010
Received in revised form 17 October 2010
Accepted 6 November 2010
Available online 13 November 2010

Keywords:
Bismuth oxyiodide
Visible-light-driven photocatalyst
Reaction mechanism

ABSTRACT

BiOI photocatalyst was synthesized by a precipitation–filtration process and consequent hydrothermal treatment. The as-prepared BiOI exhibits efficient photocatalytic activity on the decomposition of widely used model pollutants, methyl orange (MO) and phenol, under visible light irradiation. Even under the illumination of a compact fluorescent lamp, the obtained BiOI also exhibits high photocatalytic activity. The possible photodegradation mechanism was studied by the examination of active species $HO^{\bullet}$, h_{vb}^{+}, or $O_2^{-\bullet}$ anions through adding scavengers such as *tert*-butanol (*t*-BuOH), I^{-} anion, bromate anion and benzoquinone (BQ). The results show that photodegradation of MO molecules is attributed to the action of h_{vb}^{+} via direct hole oxidation process and the oxidation action of the generated $O_2^{-\bullet}$ radicals. Dissolved oxygen play an important role in photocatalytic reaction, which could trap the photogenerated electrons to reduce the recombination of h_{vb}^{+} and e_{cb}^{-} and also function as a precursor of main oxidant $O_2^{-\bullet}$. Hydroxyl radical was verified to be inappreciable for the decomposition of MO.

1. Introduction

Nowadays, two of the most urgent issues facing modern society are the depletion of energy resources and the deterioration of the natural environment. Semiconductor-based photocatalysis is attracting extensive interest as a kind of "green" technology to alleviate both the problems by splitting water for green energy hydrogen production and degrading toxic pollutants [1,2]. However, the widely used photocatalyst TiO_2 is only active in the UV range [3], so developing more efficient visible-light-driven photocatalysts is indispensable. Although dye sensitization or doping of other elements makes the utilization of visible light possible [4–7], stable and efficient dyes are rare while dopants act usually as a recombination centers for the photogenerated electrons and holes. Therefore, many researchers focus their efforts on the design and development of new single-phase effective photocatalysts under visible light irradiation.

Recently, the Bi-based layered structure compounds, including Aurivillius family [8–10], Sillén family [11–13] and Aurivillius–Sillén intergrows [14], have been extensively investigated as visible-light-driven photocatalysts due to their unique layered structure and high activity. It is believed that the formed internal electric fields between the slabs are beneficial to inducing the efficient separation of photogenerated electron-hole pairs and then improving the photocatalytic activity of the catalysts [15]. BiOI, belonging to the Sillén family expressed by $[M_2O_2][I_m]$ ($m=2$), has drawn increasing attention for the application as photocatalyst owing to its small band gap (1.77–1.92 eV) and strong absorption in visible-light region. Up to now, different morphologies of BiOI, such as 3D hierarchical structures [16–18], nanosheets [19,20] and nanolamellas [21] have been fabricated successfully by a variety of methods, and various model pollutants, including methyl orange (MO), methylene blue (MB), rhodamine (RhB), sodium pentachlorophenol (PCP-Na) and phenol, have been used to evaluate their photocatalytic activity. Among them, Lei et al. fabricated BiOI with 3D flower-like hierarchical structure and investigated its formation process and photocatalytic activity on the degradation of organic dye pollutants [17]. Xiao et al. obtained more uniform 3D BiOI microspheres in ethanol–water mixed solvent and studied its self-assembled mechanism and visible light photocatalytic activity for the degradation and mineralization of phenol [18]. Although many investigations have been performed on the preparation and photocatalytic activity of BiOI, only Chang's group [20] investigated the photocatalytic mechanism of BiOI nanosheets and systematic research on photodegradation mechanism of BiOI is lack. In addition, considering the future practical application it is still in need of studies on enhancing the photocatalytic activity of BiOI.

In the filed of photocatalysis, it is generally accepted that the photodegradation of dyes and organic pollutants has been proceeded via photocatalytic oxidation (PCO) process. The primary reactive species (RS) involved in PCO process include RS_{ads} on surface of photocatalyst (h^{+},$^{\bullet}OH_{ads}$) and RS_{free} in solution ($O_2^{-\bullet}$, $^{\bullet}OH_{free}$, H_2O_2). However, so far, whether photoreaction occurs on

* Corresponding author. Tel.: +86 371 67781019; fax: +86 371 67781558.
E-mail address: lizhongjun@zzu.edu.cn (Z. Li).

1381-1169/$ – see front matter © 2010 Elsevier B.V. All rights reserved.
doi:10.1016/j.molcata.2010.11.005

the catalyst surface or in the solution has long been continuous controversy, and the behaviors of different active species in the various stages of photocatalysis are not clear. It is also the case for the photocatalysis of BiOI.

In the present work, we synthesized BiOI photocatalyst with highly enhanced photocatalytic activity by a precipitation–filtration process and consequent hydrothermal treatment. Phenol and MO were chosen as model pollutants to evaluate the photocatalytic performance of the BiOI samples. Various free radical scavengers were introduced to the photocatalytic reaction system to explore the behaviors of different reactive species and the reaction mechanism underlying.

2. Experimental

2.1. Sample preparation

All the reagents were of AR grade and were used without further purification. In a typical synthesis, 5 mmol $Bi(NO_3)_3{\cdot}5H_2O$ was dissolved in 10 mL 3 mol L^{-1} HNO_3. 2 mol L^{-1} NaOH solution was added dropwise to adjust the pH value of the solution to 3.0 under vigorous stirring. The mixture was stirred for 0.5 h at room temperature in air. The resulting precursor precipitates were filtrated and washed with deionized water thoroughly, and then transferred to a 100 mL Teflon-lined autoclave together with 10 mmol KI. The deionized water was added up to 70% of the total volume. After being further stirred for 0.5 h, the autoclave was sealed in a stainless steel tank and heated at 160 °C for 12 h under autogenously pressure, and then air cooled to room temperature. The resulting precipitates were filtrated and washed with ethanol and deionized water thoroughly and dried at 80 °C in air.

For the purpose of comparison, BiOI powders were also prepared by a chemical precipitation reaction following the previous study [22], the product was named as PR-BiOI.

2.2. Characterization

The X-ray diffraction (XRD) patterns of the samples were measured on an X'Pert PRO X-ray powder diffractometer with Cu-Kα radiation (λ = 1.5418 Å). The morphology of the samples was investigated by scanning electron microscopy (SEM, Zeiss EVO LS-15), transmission electron microscopy (TEM, Tecnai G^2 20 S-TWIN) and high resolution transmission electron microscopy (HRTEM, JEOL JEM-2100). UV–vis diffuse reflectance spectra (DRS) were obtained using a UV–vis spectrometer (Shimadzu U-3010) by using $BaSO_4$ as a reference. Nitrogen adsorption–desorption isotherms were collected on a NOVA 1000e surface area and porosity analyzer (Quantachrome, USA) at 77 K after the sample had been degassed in the flow of N_2 at 150 °C for 1.5 h. The BET surface area was estimated using desorption data.

2.3. Photocatalytic activity test

The photocatalytic performance of the as-prepared samples was characterized by decomposing methyl orange (MO) or phenol under visible light irradiation at room temperature. A 500 W Xe-illuminator was used as a light source, 2 mol L^{-1} $NaNO_2$ solution to eliminate UV light (cutoff λ < 400 nm) [1]. The photodegradation experiments were carried out with the samples (500 mg) suspended in MO or phenol aqueous solution (500 mL, 10 mg L^{-1} and 20 mg L^{-1}, respectively) with constant stirring. Prior to the irradiation, the suspensions were magnetically stirred in the dark for 1 h to establish the adsorption/desorption equilibrium. At the given time intervals, about 5 mL of the suspension was taken for analysis after centrifugation. The concentration of MO was detected by measuring the absorption intensity at a wavelength of 464 nm. The absorption intensity was converted to the MO concentration referring to a standard curve which showed a linear relationship between the concentration and the absorption intensity. The concentration of phenol was estimated by measuring the absorption at a wavelength of 510 nm using the colorimetric method of 4-aminoantipyrine [23].

To investigate the possibility of practical application, a U-type compact fluorescent lamp (Philips Genie energy saving lamp, 23 W) was also selected as a light source for the degradation of MO.

In experiments requiring scavengers, the calculated amount of scavengers was introduced into the MO solution before the addition of the catalyst. For experiments with purging nitrogen gas, the flow rate of nitrogen gas was controlled at 0.4 L min^{-1}. Before the experiments, nitrogen gas was purged for 30 min to give the desired oxygen level.

Terephthalic acid, which reacts readily with $OH^{\bullet}$ to produce a highly fluorescent product, 2-hydroxyterephthalic acid, was employed as a probe molecule to detect the formed hydroxyl radicals ($OH^{\bullet}$) [24]. The fluorescence intensity around 425 nm, which can be ascribed to the characteristic of 2-hydroxyterephthalic acid, is proportional to the amount of hydroxyl radicals formed in solution. The detection experiment process is similar to the photodegradation experiment, with the exception of a basic terephthalic acid solution instead of MO or phenol suspension. The concentration of terephthalic acid was set at 5×10^{-4} mol L^{-1} in a dilute NaOH (2×10^{-3} mol L^{-1}) solution. The sampling was carried out every 15 min, and the withdrawn solution was measured on a Hitachi F-4500 fluorescence spectrophotometer after centrifugation. The excitation wavelength used was 315 nm.

3. Results and discussion

3.1. Characterizations of the BiOI samples

The morphology and microstructure of the BiOI samples was revealed by the SEM and TEM images (Fig. 1). The as-prepared samples have a 3D hierarchical structures constructed by nanoplates (Fig. 1a), the size of which can be estimated to be about 250–500 nm by the TEM investigation as shown in Fig. 1b. The as-prepared photocatalysts possess 3D hierarchical architectures, which will be beneficial to the separation of electron–holes and therefore improving the photocatalytic activity. In addition, the photocatalysts with hierarchical structures are more easily separated and recycled from the practical point of view [25].

Fig. 2 presents the XRD patterns of the BiOI samples before and after photocatalytic reaction. The as-prepared BiOI is well crystallized in a single phase, all of the diffraction peaks can be indexed to the tetragonal phase BiOI (space group P4/nmm, JCPDS 10-0445). No other impurities can be detected. The intense and narrow diffraction peaks reveal the good crystallinity of the BiOI samples. The standard intensity of the (1 1 0) peak is much weaker than that of the (1 0 2) peak, which could be expressed as $I(1\,1\,0)/I(1\,0\,2) = 0.55$. In our case, the intensity of the (1 1 0) peak is close to that of (1 0 2) peak, the value of $I(1\,1\,0)/I(1\,0\,2)$ was increased to 0.98. The related high-resolution TEM (HRTEM) images of a single nanoplate from as-prepared BiOI sample are shown in Fig. 1c and d, which display clearly resolved crystalline domain with a uniform interplanar spacing of 0.282 nm, corresponding well to the (1 1 0) plane of the tetragonal phase BiOI (JCPDS 10-0445). It indicates that the BiOI anisotropic grew along the (1 1 0) plane, which is in good agreement with the results of XRD.

The UV–vis diffuse reflectance spectrum of the as-synthesized BiOI samples is shown in Fig. 3. The absorption edge of the samples extends nearly to the whole spectra of visible light, ranging from 200 nm to 600 nm. The obvious absorption edge is located at about

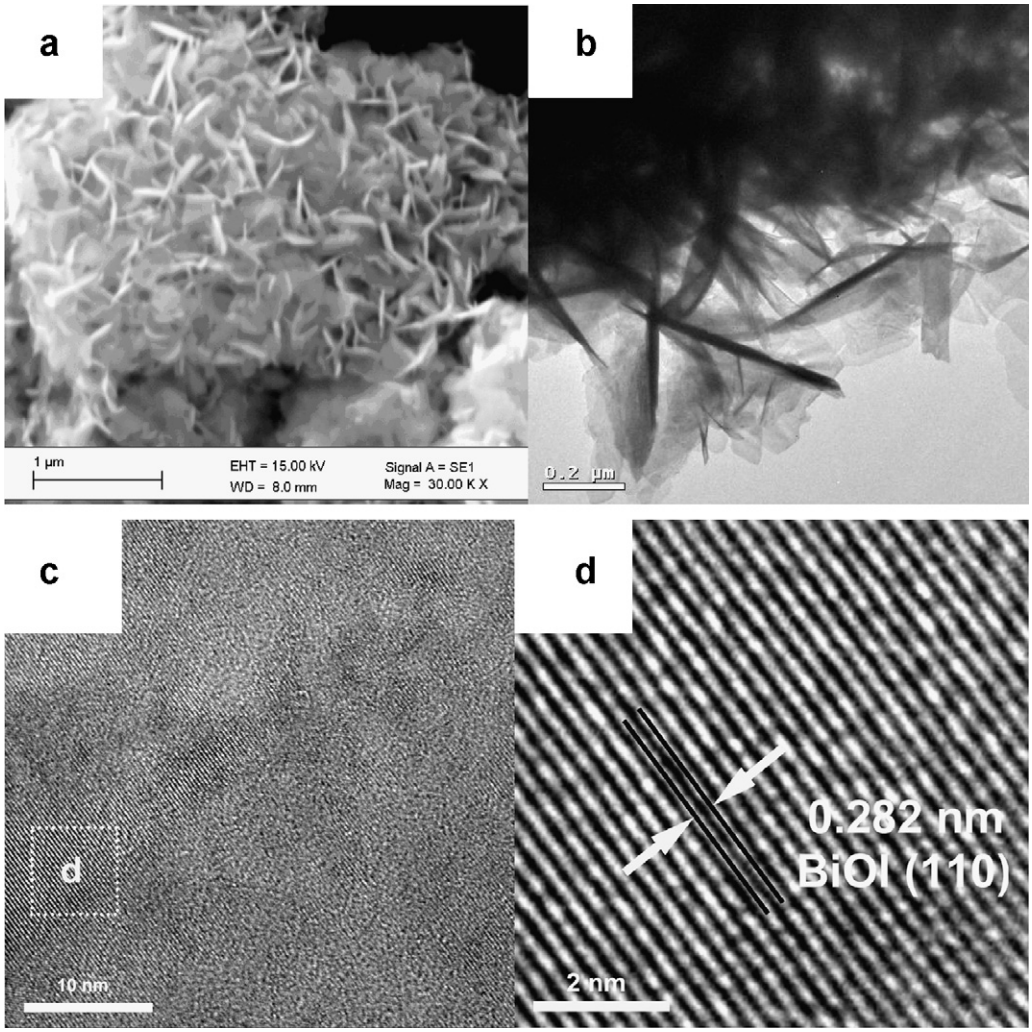

Fig. 1. (a) SEM and (b) TEM images of the as-prepared BiOI samples; (c) high-resolution TEM investigation of a single nanoplate from as-prepared BiOI samples and (d) the enlarged image of the HRTEM investigation.

640 nm in the visible light region. Considering BiOI to be an indirect semiconductor [16,26], plot of $(\alpha h\nu)^{1/2}$ versus $h\nu$ affords the band gap of BiOI as shown in the inset of Fig. 3 (where α and ν are the absorption coefficient and light frequency, respectively), and then

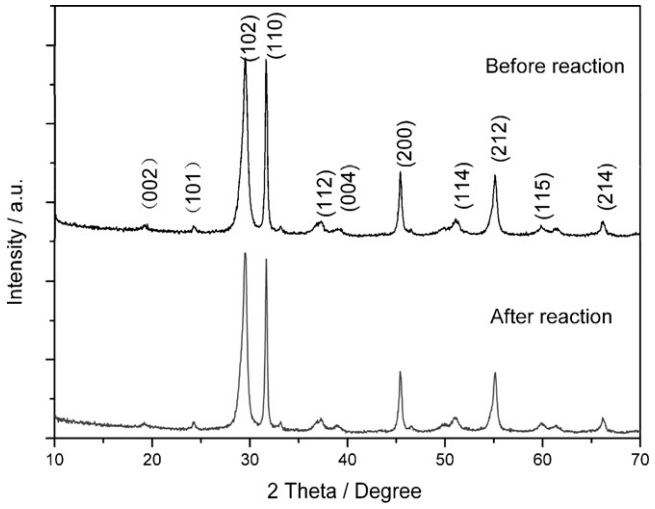

Fig. 2. XRD patterns of the BiOI samples before and after photocatalytic reaction.

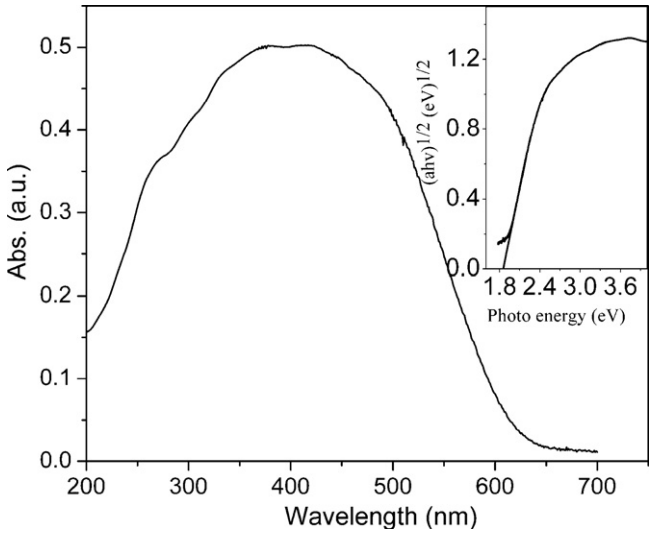

Fig. 3. The diffuse reflection spectrum of as-prepared BiOI samples. The inset is the $(\alpha h\nu)^{1/2}$–$h\nu$ curve.

evaluate the band gap E_g by extrapolating the straightest line to the $h\nu$ axis intercept. The estimated band gap energy of the resulting samples is about 1.85 eV. The steep shape of the visible edge and the strong absorption in the visible region reveal that the absorption bands of BiOI are ascribed not to the transition from the impurity to the conduction band but to the intrinsic transition between the valence band and the conduction band.

The specific surface area and porosity of the BiOI samples were investigated by using nitrogen adsorption and desorption isotherms. The isotherms can be categorized as type IV with a distinct hysteresis loop observed in the range of 0.8–1.0p/p_0, indicating the presence of mesopores in the size range of 2–50 nm (Fig. 4). The pore-size distribution obtained from the isotherm indicates that the pore diameters are mainly located at about 17.6 nm besides plenty of micropores (inset in Fig. 4). These mesopores are believed to be produced by interaggregated BiOI plates in the microparticles. The BET specific surface area of the sample is calculated from N_2 isotherms and is found to be as much as 22.3 $m^2\ g^{-1}$.

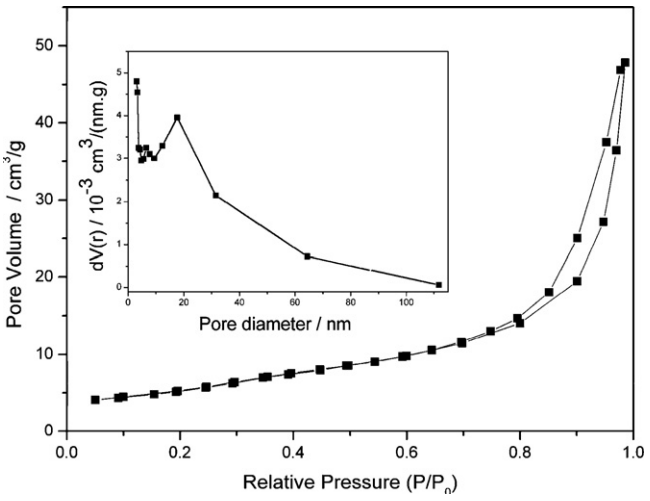

Fig. 4. N_2 adsorption and desorption isotherms and pore-size distribution (inset) for the BiOI samples.

3.2. Photocatalytic performance

Azobenzene dye methyl orange (MO) was chosen as a representative model pollutant to evaluate the photocatalytic performance of samples. Fig. 5a illustrates temporal evolution of the spectral changes during photodegradation of MO over as-prepared BiOI samples under visible light illumination. The band at 464 nm, which is attributed to the azo bond (–N=N–), was used to monitor the photocatalytic degradation process. It can be seen that the absorbance at 464 nm decreased markedly with irradiation time and almost completely disappeared after 50 min of irradiation, which indicates destruction of the conjugated structure occurred. Fig. 5b shows the photocatalytic performances of different photocatalysts on degradation of MO. The photolysis of MO is extremely slow and only 2% of MO is degraded after 60 min under visible-light irradiation. The degradation of MO with as-prepared BiOI samples in the dark condition gives similar results to the photolysis test, indicating that the adsorption of MO on the BiOI samples is

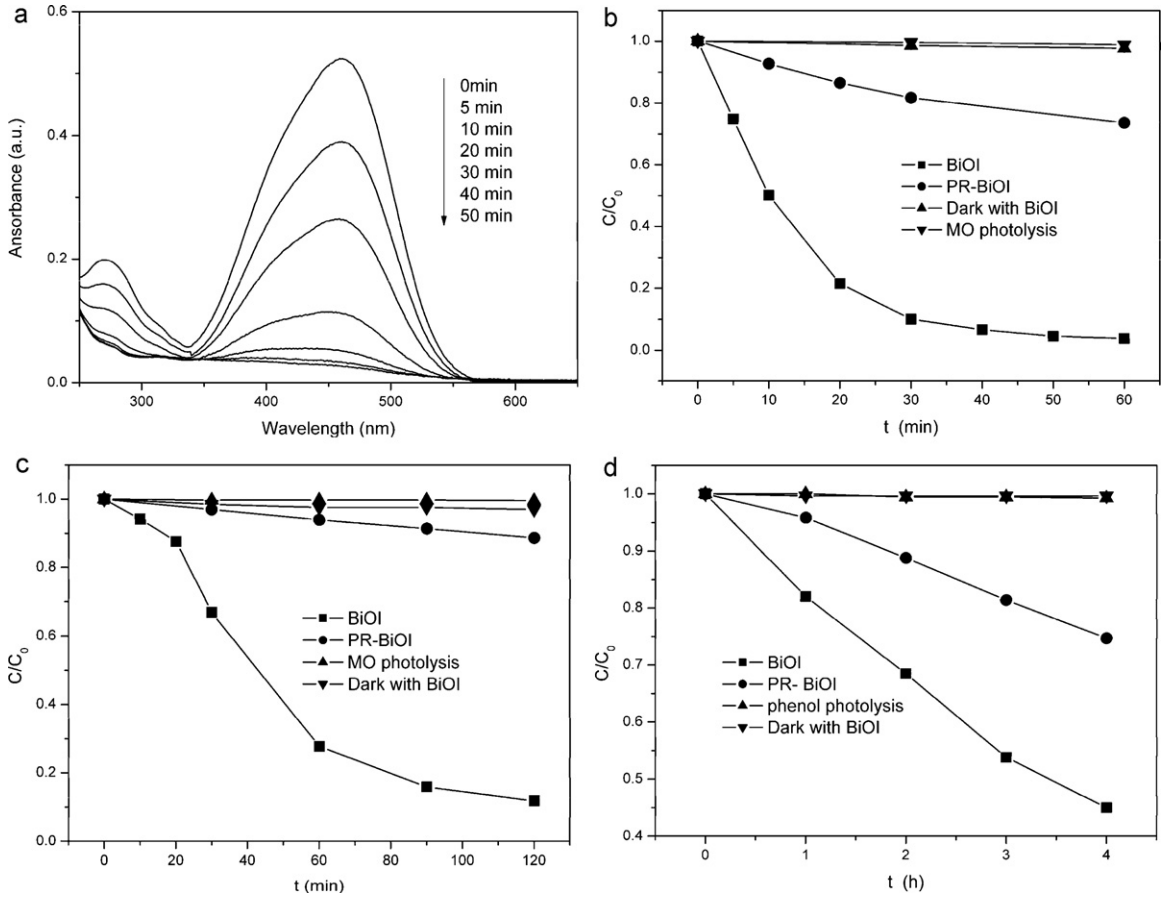

Fig. 5. (a) UV–vis spectral changes of MO in the presence of as-prepared BiOI as a function of visible light illumination time; (b) comparison of the photocatalytic degradation of MO in the presence of different catalysts; (c) photocatalytic activity of BiOI under the U-type compact fluorescent lamp and (d) photodegradation efficiencies of phenol as a function of irradiation time.

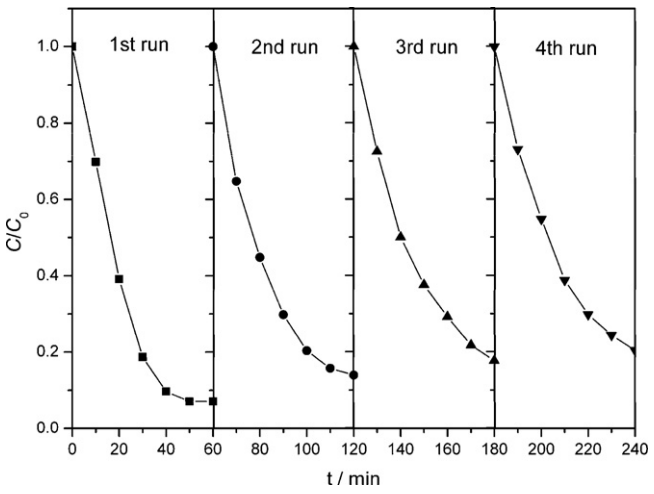

Fig. 6. Cycling runs in photocatalytic degradation of MO in the presence of BiOI samples.

limited after the adsorption–desorption equilibrium was reached. However, about 97% of MO is decolorized after 60 min over as-prepared BiOI photocatalyst, exhibiting efficient photocatalytic activity under visible-light irradiation ($\lambda > 400$ nm). Although there might be photolysis for MO [27], the results of above comparison signify that MO degradation in the present study is through a photocatalytic process. For comparison, the photocatalytic property of PR-BiOI is also tested. After 60 min under visible-light irradiation, the degradation efficiency of MO is only 26%, which is significantly less than that of as-prepared BiOI samples under the same conditions.

A 23 W U-type compact fluorescent lamp was also used as a light source. Fig. 5c demonstrates the photocatalytic activity of BiOI is also high under this condition. After 120 min of irradiation, the photodegradation efficiency of BiOI reaches nearly 88%, which is much higher than that of PR-BiOI. These results are very beneficial to future practical applications, because changing the light resource from 500 W Xe-illuminator to 23 W compact fluorescent lamp did not affect the photodegradation efficiency obviously, while the power consumption is decreased sharply. In the practical application of photocatalysis, the consuming of the power is still a problem to be solved. The as-prepared BiOI sample exhibits high photocatalytic ability under indoor lighting condition, which brings the hope to its future application.

As it is hard to avoid the decoloring of dyes from adsorption and photosensitization, the other widely adopted organic pollutant phenol was also used to evaluate the photocatalytic performance of samples. In the absence of any scavenger agent, the photodegradation efficiency of phenol over BiOI (seen from Fig. 5d) reaches about 55% after 4 h of irradiation. The PR-BiOI exhibited a much poorer effect compared to the as-prepared BiOI under the same conditions. Meanwhile, no degradation of phenol was observed without the catalyst or without the light. The results obtained indicate that the BiOI sample also exhibit excellent photocatalytic performance on degradation of phenol.

To test the stability and reusability of BiOI samples, the circulating runs in the photocatalytic degradation of MO in the presence of BiOI under visible light irradiation were checked. As shown in Fig. 6, BiOI sample still exhibited effective degradation on MO after four cycles and the photocatalytic efficiency decreases only 13%. Additionally, the XRD pattern of BiOI after photocatalytic reaction shown in Fig. 2 reveals that the phase and structure remain intact. These results indicate that the as-prepared BiOI has high stability during photocatalytic oxidation of model pollutant.

3.3. Photocatalytic mechanism

3.3.1. Effects of scavengers and N_2 purging

The excellent photocatalytic performance of the as-prepared BiOI motivated us to further investigate the underlying photocatalytic mechanism. The effects of some radical scavengers and N_2 purging on the degradation of MO were examined in an attempt to elucidate the reaction mechanism. As an $OH^\bullet$ scavenger, excess *t*-BuOH was added to the reaction system [28,29], and iodide was introduced as the scavenger of VB hole and $OH^\bullet$ [30,31]. Bromate, which is a strong oxidant [32,33], was used as a CB electron acceptor replacing oxygen. Benzoquinone (BQ) was adopted to quench $O_2^{-\bullet}$ to explore the role of dissolved oxygen [30]. Continuous N_2 purging, or air equilibrium conditions (i.e., no gas purging) was employed depending on the experimental objective.

Effect of hydroxy radical and valence band hole Iodide ion is a scavenger and reacts with $^\bullet OH_{ads}$ and h_{vb}^+ [32,34], as shown in Eqs. (1)–(5).

$$I^- + {}^\bullet OH_{ads} \rightarrow I^\bullet + OH_{ads}^- \quad (1)$$

$$I^- \rightarrow I^\bullet + e^- \quad (2)$$

$$e^- + h_{vb}^+ \rightarrow \text{heat} \quad (3)$$

$$I^\bullet + I^- \rightarrow I_2^{-\bullet} \quad (4)$$

$$I_2^{-\bullet} \leftrightarrow I_2 + e^- \quad (5)$$

As can be seen from Fig. 7a, the addition of excess KI (10 mM) inhibited significantly the decomposition of MO compared with no scavenger at the same conditions, indicating that the h_{vb}^+ and/or $^\bullet OH_{ads}$ pathways have a crucial role in the process of MO oxidation. Since both h_{vb}^+ and $^\bullet OH_{ads}$ are the reactive species on the surface of photocatalysts, the degradation of MO takes place on the surface of photocatalyst not in the bulk solution, mediated chiefly by the action of h_{vb}^+ and/or $^\bullet OH_{ads}$. The degradation of MO was further suppressed under N_2-purging compared with air-equilibrated conditions. This is related to the effect of dissolved oxygen which will be discussed in the following section.

t-BuOH can react quickly with $^\bullet OH$ with a rate constant of $6.0 \times 10^8\ M^{-1}\ s^{-1}$ [35], as shown in Eq. (6)

$$t\text{-BuOH} + {}^\bullet OH \rightarrow t\text{-BuO}^\bullet + H_2O \quad (6)$$

Excess *t*-BuOH (10 mM) was added to the solution to scavenger all the hydroxyl radicals produced in the system. If the hydroxyl radicals play a major role in the decolorization of MO, the reaction rate is expected to be greatly decreased. As shown in Fig. 7a, however, excess *t*-BuOH showed a negligible effect on the photocatalytic oxidation of MO, indicating $^\bullet OH$ was not involved in the phototransformation of MO. The results are consistent with the previous reports on the degradation of dyes [20,30].

To further research the effect of $^\bullet OH$, the PL technique was employed to detect the $^\bullet OH$ formed on the surfaces of photocatalysts. For comparison, P25 was also tested as a reference. Fig. 7c and d shows the fluorescence spectral changes observed during light irradiation of P25 and BiOI in a basic terephthalic acid solution (excitation wavelength at 315 nm). As shown, the PL intensity around 425 nm gradually increased with the irradiation time for P25, which demonstrates the production of the hydroxyl radicals [24]. However, in the case of BiOI sample, no photofluorescence was observed, demonstrating that no hydroxyl radicals were formed during the photodegradation process. These results confirm that hydroxyl radicals do not dominate the photodegradation procedure of BiOI sample. Combining the above, it can be concluded that the conversion of MO is dominated by the h_{vb}^+ pathway rather than $^\bullet OH_{ads}$ reactions taking place on the surface of photocatalyst.

Effect of dissolved oxygen Although $^\bullet OH$ radicals mediated pathway and hole mechanism are generally deemed to dominant in

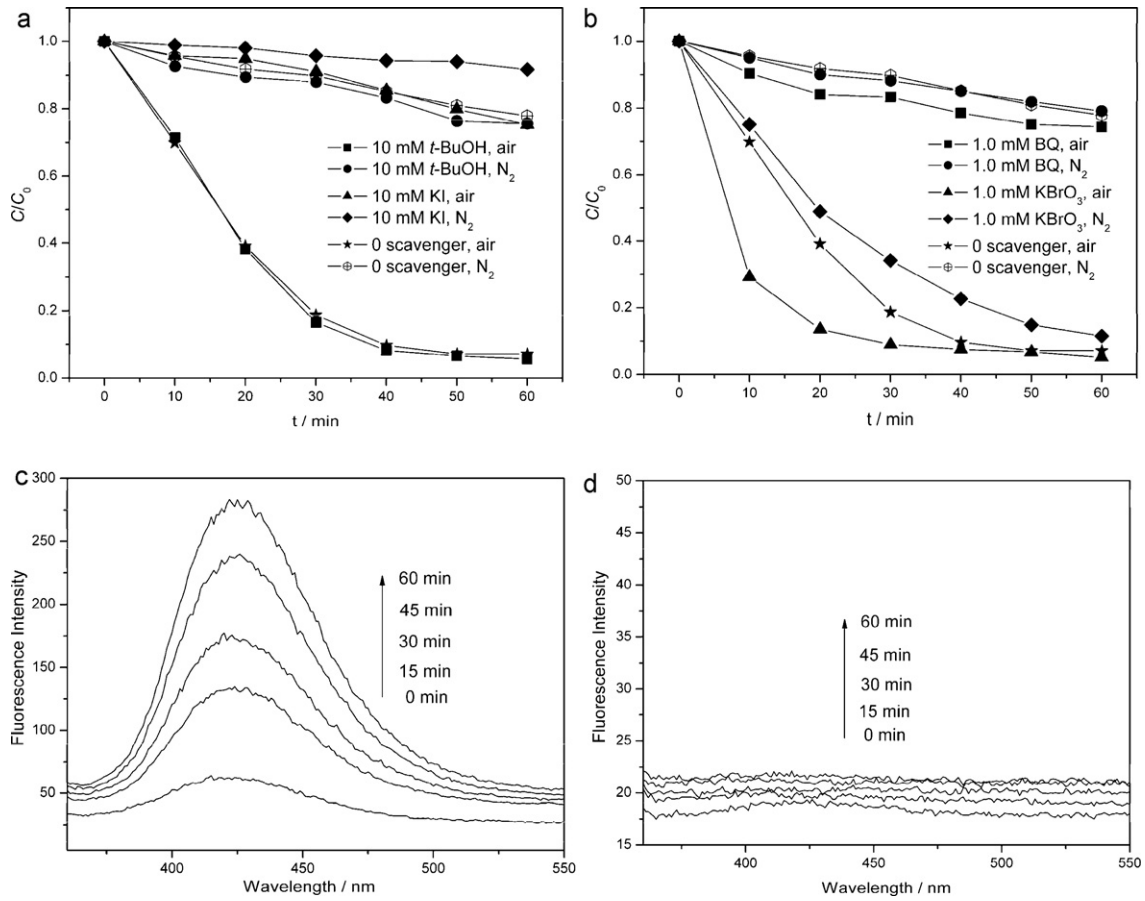

Fig. 7. (a) Effects of I^- and *t*-BuOH on degradation of MO in the presence of BiOI under visible light irradiation; (b) effects of BrO_3^- and BQ on degradation of MO in the presence of BiOI under visible light irradiation; fluorescence spectral changes observed during irradiation of P25 (c) and BiOI (d) in a basic solution of terephthalic acid.

most photocatalytic oxidation reactions [36–38], superoxides have been recently proposed as a main photocatalytic oxidants in photocatalytic oxidation of some metal ions and azo-dye [39,40]. To investigate the effects of dissolved oxygen, N_2 purging experiment was conducted compared with air-equilibrated condition. Seen from Fig. 7a, as N_2 purging was conducted (0 scavenger), the decolorization rate of MO was remarkably decreased compared with air-equilibrated conditions (0 scavenger), which shows that dissolved oxygen is significant to MO decolorization.

To further examine the roles of dissolved oxygen, excess BrO_3^- (1.0 mM), proved to be an effective electron acceptor, was added to trap the photogenerated electrons. The addition of $KBrO_3$ enhanced the photocatalytic efficiency of MO (seen from Fig. 7b), suggesting that BrO_3^- does accelerate the separation of e_{cb}^-–h_{vb}^+ in photocatalysts and the hole over the photocatalyst is responsible for the conversion of MO. The dissolved oxygen is universally regarded as a conduction band electrons scavenger to inhibit fast carrier recombination. However, instead of dissolved oxygen, the addition of excess BrO_3^- with N_2 purging had lower photocatalytic efficiency of MO compared with no scavenger under air-equilibrated condition. Therefore, dissolved oxygen not only functions as a conduction band electrons scavenger but, more importantly, may act as a precursor of main oxidant.

Dissolved oxygen can act as a photogenerated electron scavenger to give $O_2^{-\bullet}$ and $^\bullet OH$ active species, the latter has been proven not to be the major oxidation species in this process. In order to examine the role of $O_2^{-\bullet}$, BQ (1.0 mM) was used as an $O_2^{-\bullet}$ quencher. Seen from Fig. 7b, the addition of BQ could greatly decrease the photocatalytic efficiency of MO at air-equilibrated condition, which shows that the MO photodegradation is caused by $O_2^{-\bullet}$ to a large degree, while the negligible effect of BQ is ascribed to absence of $O_2^{-\bullet}$ in solution at N_2 purging condition. These observations confirm the proposed assumption that dissolved oxygen is a precursor of main oxidant, that is, the role of dissolved oxygen is to trap the photogenerated electrons to produce $O_2^{-\bullet}$ radicals, which participate in photocatalytic process to accelerate the MO photodegradation.

In summary, MO molecules were decolorized on the surface of photocatalyst by photocatalytic process. According to the effects of scavengers, the decomposition of MO molecules was attributed to the action of h_{vb}^+ via direct hole oxidation process and the oxidation action of the generated $O_2^{-\bullet}$ radicals. Dissolved oxygen could trap the photogenerated electrons to reduce the recombination of h_{vb}^+ and e_{cb}^- in concert with the formation of $O_2^{-\bullet}$ radicals oxidant. Hydroxyl radical was verified to be insignificant for the decomposition of MO.

3.3.2. *Band gap structures and possible degradation mechanism*

The valence band potentials of BiOI were estimated in this study according to the following empirical equation:

$$E_{VB} = X - E^e + 0.5\,E_g \quad (7)$$

where E_{VB} is the valence band edge potential, X is the electronegativity of the semiconductor, which is the geometric mean of the electronegativity of the constituent atoms, and the value of X for BiOI is ca. 5.99 eV, E^e is the energy of free electrons on the hydrogen scale (about 4.5 eV), E_g is the band gap energy of the semiconductor. Following Eq. (7), the E_{VB} of BiOI was calculated to be 2.42 eV. E_{CB} (conduction band edge potential) can be determined by $E_{CB} = E_{VB} - E_g$. The band gap of the as-prepared BiOI

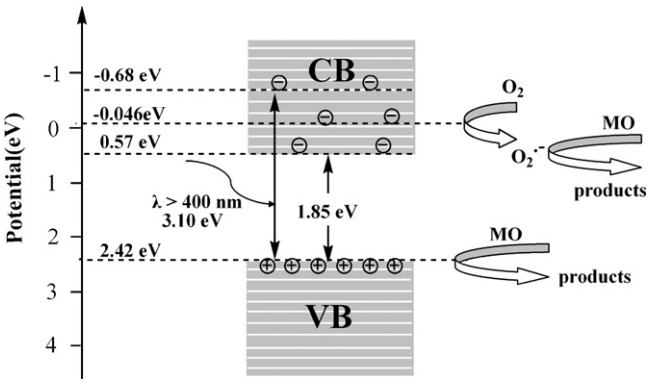

Scheme 1. Illustration of band gap structure of BiOI and the simplified pathways for photocatalytic degradation of MO.

sample is about 1.85 eV, thus, the E_{CB} of BiOI was estimated to be 0.57 eV.

On the base of band gap structure of BiOI and the effects of scavengers, a possible pathway for the photocatalytic degradation of MO with BiOI photocatalyst (Scheme 1) was proposed as follows:

$$BiOI + h\nu(\lambda < 400\,nm) \rightarrow BiOI(e_{cb}^- + h_{vb}) \quad (8)$$

$$BiOI(e_{cb}^-) + O_2 \rightarrow BiOI + O_2^{-\bullet} \quad (9)$$

$$h_{vb}^+ + MO \rightarrow \text{degradationproduct} \quad (10)$$

$$O_2^{-\bullet} + MO \rightarrow \text{degradationproduct} \quad (11)$$

The MO molecules to be degraded adsorb preferentially on the surface of photocatalyst, and are tacked by h_{vb}^+ and transformed to degradation products via the direct hole oxidation pathway. The MO is also eliminated by oxygenous radical oxidation under visible light irradiation to a large degree.

4. Conclusions

In conclusion, visible-light-induced BiOI photocatalyst was synthesized successfully by a precipitation–filtration process and subsequent hydrothermal treatment. The as-obtained BiOI samples exhibits excellent performance on the degradation of MO and phenol under visible light irradiation. Even under the irradiation of a 23 W U-type compact fluorescent lamp, BiOI samples also exhibits efficient photocatalytic activity on decomposing MO. Photocatalytic mechanism investigations demonstrate that the degradation of MO over the as-prepared BiOI catalysts under visible light is mainly via the direct hole oxidation mechanism and superoxide oxidation pathway.

Acknowledgements

This work was supported by the Project Nos. 20971111 and 21001096 of National Natural Science Foundation of China.

References

[1] K. Maeda, T. Takata, M. Hara, N. Saito, Y. Inoue, H. Kobayashi, K. Domen, J. Am. Chem. Soc. 127 (2005) 8286–8287.
[2] A. Hameed, T. Montini, V. Gombac, P. Fornasiero, J. Am. Chem. Soc. 130 (2008) 9658–9659.
[3] D. Zhang, G. Li, X. Yang, J.C. Yu, Chem. Commun. (2009) 4381–4383.
[4] W.R. McNamara, R.C. Snoeberger, G. Li, J.M. Schleicher, C.W. Cady, M. Poyatos, C.A. Schmuttenmaer, R.H. Crabtree, G.W. Brudvig, V.S. Batista, J. Am. Chem. Soc. 130 (2008) 14329–14338.
[5] H. Hagiwara, N. Ono, T. Inoue, H. Matsumoto, T. Ishihara, Angew. Chem. 118 (2006) 1448–1450.
[6] S. Livraghi, M.C. Paganini, E. Giamello, A. Selloni, C. Di Valentin, G. Pacchioni, J. Am. Chem. Soc. 128 (2006) 15666–15671.
[7] X. Sun, J. Lin, J. Phys. Chem. C 113 (2009) 4970–4975.
[8] H.G. Kim, D.W. Hwang, J.S. Lee, J. Am. Chem. Soc. 126 (2004) 8912–8913.
[9] Y. Shimodaira, H. Kato, H. Kobayashi, A. Kudo, J. Phys. Chem. B 110 (2006) 17790–17797.
[10] D. Ma, S. Huang, W. Chen, S. Hu, F. Shi, K. Fan, J. Phys. Chem. C 113 (2009) 4369–4374.
[11] X. Lin, T. Huang, F. Huang, W. Wang, J. Shi, J. Phys. Chem. B 110 (2006) 24629–24634.
[12] Z. Ai, W. Ho, S. Lee, L. Zhang, Environ. Sci. Technol. 43 (2009) 4143–4150.
[13] K.L. Zhang, C.M. Liu, F.Q. Huang, C. Zheng, W.D. Wang, Appl. Catal. B: Environ. 68 (2006) 125–129.
[14] X. Lin, T. Huang, F. Huang, W. Wang, J. Shi, J. Mater. Chem. 17 (2007) 2145–2150.
[15] S. Sun, W. Wang, L. Zhang, L. Zhou, W. Yin, M. Shang, Environ. Sci. Technol. 43 (2009) 2005–2010.
[16] X. Zhang, Z. Ai, F. Jia, L. Zhang, J. Phys. Chem. C 112 (2008) 747–753.
[17] Y. Lei, G. Wang, S. Song, W. Fan, M. Pang, J. Tang, H. Zhang, Dalton Trans. 39 (2010) 3273–3278.
[18] X. Xiao, W.D. Zhang, J. Mater. Chem. 20 (2010) 5866–5870.
[19] H.Z. An, Y. Du, T.M. Wang, C. Wang, W.C. Hao, J.Y. Zhang, Rare Met. 27 (2008) 243–250.
[20] X. Chang, J. Huang, Q. Tan, M. Wang, G. Ji, S. Deng, G. Yu, Catal. Commun. 10 (2009) 1957–1961.
[21] F. Fang, L. Chen, L.M. Wu, Chin. J. Struct. Chem. 28 (2009) 1399–1406.
[22] W. Wang, F. Huang, X. Lin, J. Yang, Catal. Commun. 9 (2008) 8–12.
[23] C. Chen, M. Long, H. Zeng, W. Cai, B. Zhou, J. Zhang, Y. Wu, D. Ding, D. Wu, J. Mol. Catal. A: Chem. 314 (2009) 35–41.
[24] H. Cheng, B. Huang, Y. Dai, X. Qin, X. Zhang, Langmuir 26 (2010) 6618–6624.
[25] Y. Li, J. Liu, X. Huang, G. Li, Cryst. Growth Des. 7 (2007) 1350–1355.
[26] W.L. Huang, J. Comput. Chem. 30 (2009) 1882–1891.
[27] W. Zhao, Z. Wu, H. Shi, D. Wang, J. Photochem. Photobiol. A: Chem. 171 (2005) 97–106.
[28] Z. He, L. Xie, J. Tu, S. Song, W. Liu, Z. Liu, J. Fan, Q. Liu, J. Chen, J. Phys. Chem. C 114 (2010) 526–532.
[29] Y. Ou, J.D. Lin, H.M. Zou, D.W. Liao, J. Mol. Catal. A: Chem. 241 (2005) 59–64.
[30] M. Yin, Z. Li, J. Kou, Z. Zou, Environ. Sci. Technol. 43 (2009) 8361–8366.
[31] S. Song, L. Xu, Z. He, J. Chen, X. Xiao, B. Yan, Environ. Sci. Technol. 41 (2007) 5846–5853.
[32] S.H. Yoon, J.H. Lee, Environ. Sci. Technol. 39 (2005) 9695–9701.
[33] Y. Oosawa, M. Gratzel, J. Chem. Soc. Faraday Trans. 1: Phys. Chem. Condens. Phases 84 (1988) 197–205.
[34] G. Li, J. Qu, X. Zhang, H. Liu, H. Liu, J. Mol. Catal. A: Chem. 259 (2006) 238–244.
[35] L.H. Chia, X. Tang, L.K. Weavers, Environ. Sci. Technol. 38 (2004) 6875–6880.
[36] G. Huang, S. Zhang, T. Xu, Y. Zhu, Environ. Sci. Technol. 42 (2008) 8516–8521.
[37] P.K. Dutta, S.O. Pehkonen, V.K. Sharma, A.K. Ray, Environ. Sci. Technol. 39 (2005) 1827–1834.
[38] S.H. Yoon, S.E. Oh, J.E. Yang, J.H. Lee, M. Lee, S. Yu, D. Pak, Environ. Sci. Technol. 43 (2009) 864–869.
[39] J. Ryu, W. Choi, Environ. Sci. Technol. 38 (2004) 2928–2933.
[40] H. Lee, W. Choi, Environ. Sci. Technol. 36 (2002) 3872–3878.